



HAL
open science

Quantification of APT physical limitations on chemical composition of precipitates in Fe–Cr alloys

Constantinos Hatzoglou, Bertrand Radiguet, Gérald da Costa, Philippe Pareige, Manuel Roussel, Mercedes Hernández-Mayoral, Cristelle Pareige

► **To cite this version:**

Constantinos Hatzoglou, Bertrand Radiguet, Gérald da Costa, Philippe Pareige, Manuel Roussel, et al.. Quantification of APT physical limitations on chemical composition of precipitates in Fe–Cr alloys. *Journal of Nuclear Materials*, 2019, 522, pp.64-73. 10.1016/j.jnucmat.2019.05.022 . hal-02130691

HAL Id: hal-02130691

<https://normandie-univ.hal.science/hal-02130691>

Submitted on 16 May 2019

HAL is a multi-disciplinary open access archive for the deposit and dissemination of scientific research documents, whether they are published or not. The documents may come from teaching and research institutions in France or abroad, or from public or private research centers.

L'archive ouverte pluridisciplinaire **HAL**, est destinée au dépôt et à la diffusion de documents scientifiques de niveau recherche, publiés ou non, émanant des établissements d'enseignement et de recherche français ou étrangers, des laboratoires publics ou privés.

Quantification of APT physical limitations on chemical composition of precipitates in Fe–Cr alloys

Constantinos Hatzoglou^a, Bertrand Radiguet^a, Gerald Da Costa^a, Philippe Pareige^a, Manuel Roussel^a, Mercedes Hernandez-Mayoral^b, Cristelle Pareige^{a,*}

^a Normandie Univ, UNIROUEN, INSA Rouen, CNRS, Groupe de Physique des Matériaux, 76000, Rouen, France

^b Materials of Energy Interest Division, Technology Department, CIEMAT, Avda. Complutense 40, 28040, Madrid, Spain

A B S T R A C T

Among the different nano-features at the origin of embrittlement of Fe–Cr alloys and steels, α' precipitates play a major role in alloys with Cr content higher than about 10at.%. If Atom Probe Tomography (APT) is recognized as an efficient technique for characterizing α' precipitates, discussions remain on its ability to measure the actual composition of small particles. Two APT limitations are at the origin of these discussions: its lateral resolution (and on a smaller scale the depth resolution) and local magnification effects due to the difference in field evaporations between the matrix and the particles. In this study, the impacts of these two limitations are quantified for the first time using numerical approaches and an analytical model. This will provide an overview of the interpretation for the α' particles chemical composition experimentally measured by APT.

The results show that: (i) the major effect of local magnification is ion focussing with no mixing in the core of the particles for particle radius larger than 1 nm, (ii) lateral resolution is the main contributor to the composition bias. Depending on the lateral resolution, the core of the small particles may be diluted by matrix atoms but the dilution does not exceed 5.2 at.%. The extent of the decrease in measured Cr concentration of the particles depends on the Cr concentration difference between particles and the surrounding matrix.

1. Introduction

High Cr ferritic-martensitic steels are of interest for GEN IV reactors because of their good swelling resistance at operating temperatures, good thermal properties and low ductile-to-brittle transition temperature shift [1–3]. However, their operating window is limited at low temperature (<350–400 °C) because of embrittlement and at high temperature (>550 °C) because of creep. Among the different nano-features at the origin of embrittlement, α' precipitates play a major role in steels with Cr content higher than about 10% [4–6].

Two major techniques are used to characterise the α/α' decomposition kinetics: Small Angle Neutron Scattering (SANS) and Atom Probe Tomography (APT). Both techniques give information about size, volume fraction and composition of phases. If

they agree reasonably well on radius and matrix composition, they do not on α' composition of particles at early stage of the precipitation kinetics whatever the ageing conditions *i.e.* under thermal ageing [7,8] or under irradiation [9,10]. At early stages, APT measurements suggest that α' particles do not have the equilibrium composition [7,9,11–15] whereas the equilibrium composition is always considered for SANS data treatment.

Disagreement also exists within the APT community. Some authors consider that measuring 60 at.%Cr in α' particles 1 nm in radius is the signature of APT artefacts [14–17], others that the origin is mainly kinetic and thermodynamic [7,9,12,18–22]. Indeed, according to theory, the interphase surface energy is one of the main factors determining the Cr content of the clusters in Fe–Cr [19]. At medium driving force, when non-classical nucleation is expected, the composition of the clusters differs from equilibrium composition of the α' phase [20,23]. The study of α' precipitation kinetics performed under thermal ageing and under irradiation using APT [7,12,24] has shown that at longer ageing time or higher irradiation dose, when the particle radius exceeds 2 nm, the

equilibrium composition is reached. At early stage, when radius ranges between 1 and 2 nm, Cr content of the particles increases from 50 to 60 at.% to the equilibrium composition. These observations raise a natural question which is at the origin of the disagreement within APT and with SANS communities: could this evolution in Cr concentration be due to APT artefacts that would induce an artificial dilution of α' particles?

One way to deal with this problem is to plot the Cr concentration in α' particles with respect to their radius [7,12,24]. Nevertheless, this method poses a problem when mixing up data originating from different ageing conditions (temperature, thermal ageing and irradiation) and different alloys (different composition *i.e.* different driving force). In such a case, it is not possible to separate APT artefact origin from thermodynamic/kinetic origins. The only method remaining is to directly study and quantify the effect of APT artefacts on measured α' composition.

Since APT relies on field evaporation, artefacts may appear and artificially modify the shape and composition of the observed particles [25–29], in particular during analysis of nano-particles exhibiting a size close to the lateral spatial resolution of the technique (between 0.5 nm and 1 nm depending on the device) and a difference in field evaporation with the surrounding matrix. Artefacts or physical limitations of the technique that can alter composition measurements in the case of Fe–Cr alloys are: preferential evaporation [30], spatial resolution (mainly lateral resolution) and local magnification effects [25–29].

Because the evaporation field of Cr is lower than the Fe one, preferential evaporation of Cr atoms may occur *i.e.* Cr atoms are evaporated at DC voltage between pulses (which trigger the evaporation and the detection system) and so not quantified. Nevertheless, analysis conditions (pulse fraction and temperature) are defined so as to suppress this effect [30,31]. Under such defined analysis conditions (low temperature and high pulse fraction ~20%), the expected nominal concentration is obtained excluding any preferential evaporation to occur. Thus, two major contributors to APT chemical biases remain to be studied: (1) the spatial resolution and (2) the local magnification. The latter occurs between two phases having a difference in evaporation field. In such conditions, both phases locally develop different curvature radius leading to a difference in magnification. This leads to a modification of the ion trajectories. In this study, both of them are studied; first separately in order to estimate quantitatively the impact of each of them on the chemical composition measurements of α' particles 1 nm in radius; and lastly simultaneously. In the first section, a brief summary of APT results used in this study as a reference experimental data set is presented. In the second section, the APT chemical biases are quantified for the two cases listed above. Quantification of composition bias due to APT spatial resolution was determined using the data numerically generated according to the method developed at the Groupe de Physique des Matériaux (France) [28]. Quantification of composition bias due to local magnification effect was undertaken by two methods: modelling of field evaporation using the method developed by Vurpillot *et al.* [25,32,33] on the one hand and using the analytical model of Hatzoglou *et al.* [29,34] on the other hand. In the last section, both effects are taken into account.

2. Description of the experimental data set

In this study, we consider the experimental results obtained by Novy *et al.* [7]. Results were obtained in a Fe-20 at.% Cr alloy aged at 500 °C for 50 h, 100 h, 150 h, 240 h, 480 h, 812 h and 1067 h. Samples were analysed using an ECoTAP (Energy Compensated Tomographic Atom Probe). Fig. 1 reports the evolution of α matrix and α' particles Cr concentrations with ageing time together with the

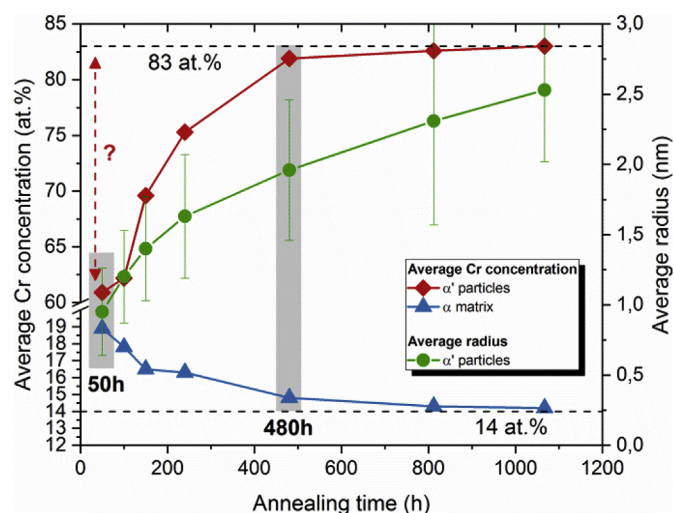


Fig. 1. Average Cr concentration (at.%) in the α matrix and the α' particles and the average radius of α' particles as a function of the annealing time (h) at 500 °C. Grey rectangles highlight the conditions that will be considered in the following.

mean particle radius. The figure shows that measured composition of α' particles increases with ageing time from 60.5 at.% to 83 at.% whereas the mean particle radius evolves from 1 nm to 2.5 nm.

The questions to answer are the following: Is it the actual evolution of the particle composition or is it due to an artificial mixing whose impact is less pronounced for large radii? Does the concentration of 60 at.% Cr measured in particles of 1 nm in radius is the actual concentration or does it result from the artificial dilution of particles having the Cr equilibrium concentration (*i.e.* between 83 at.% and 88 at.% [7,35,36]) because of limited lateral resolution and/or of local magnification effect ?

3. Quantification of chemical biases for Fe–Cr alloys due to APT spatial resolution and local magnification effects as separate effects

3.1. APT spatial resolution

The lateral resolution of APT (in the plane normal to the analysis direction) varies from about 0.2 nm to 1 nm depending on the atom probe used whereas the depth resolution is much better (~0.04–0.09 nm) [27]. In the framework of this study, the lateral resolution of both ECoTAP and LEAP HR 4000 has been measured. The spatial resolution is measured using the Fourier transform calculation of the atomic distribution [27] (when atomic planes are reconstructed, the Fourier diagram shows the presence of spots in the reciprocal space placed at the fundamental positions $1/d_{hkl}$ where d_{hkl} is the interplanar distance). Experimentally, the diffraction peaks are clearly observed but the intensity of these peaks decreases in the reciprocal space. From amplitude measurement of each observed peak, along the different directions slanted with respect to the analysis axis, it is therefore possible to extract an estimated value of both lateral and depth resolutions (Table 1). Lateral resolution of ECoTAP is better than the LEAP HR

Table 1
Measured lateral and depth resolutions (nm) of ECoTAP and LEAP HR 4000.

| Atom Probe | Lateral resolution (nm) | Depth resolution (nm) |
|--------------|-------------------------|-----------------------|
| ECoTAP | 0.35 ± 0.10 | 0.036 ± 0.001 |
| LEAP 4000 HR | 0.85 ± 0.10 | 0.051 ± 0.002 |

one. It is due to their difference in view angle. If the higher lateral resolution of ECoTAP is an advantage, the much smaller analysed volume is not.

This lateral uncertainty on the position of the atoms creates some lateral scatter which can bias the chemical composition measurements [28]. In order to study and quantify the influence of the lateral resolution on measurements, the numerical approach presented in Ref. [28] using the tool developed at the Groupe de Physique des Matériaux has been used.

Microstructures similar to the ones presented in Fig. 1 have been simulated and degraded to simulate the scatter created by both lateral and depth resolutions. Twenty particles were randomly distributed on a rigid BCC lattice ($a_0 = 0.28 \text{ nm}$) in a simulation box of size of $30 \times 30 \times 30 \text{ nm}^3$. Abrupt interfaces between the α matrix and α' particles have been simulated in order to match with the experimental observations. The cluster radius was chosen equal to 1.0 nm which corresponds to the smallest average radius experimentally observed (*i.e.* at 50 h , Fig. 1). It is indeed for the smallest size that the highest biases are expected. The Cr concentration in the matrix is set to $19 \text{ at.}\%$ which is the measured value of Cr in the matrix at 50 h [7]. Six different Cr concentrations were chosen as input for the clusters, from 40 to $90 \text{ at.}\%$ of Cr in order to evaluate the combined impact of the spatial resolution and detection efficiency on the measured Cr content of the particles. Study of the contribution of the two separately can be found in Ref. [28]. Detection efficiency of APT (Q) was also taken into account. Detector efficiency is due to the fact that not all atoms evaporated from the sample are detected [37]. The detection efficiency was simulated by randomly removing 50% for ECoTAP and 40% for LEAP HR of the atoms since detection efficiency does not depend on the chemical nature of the evaporated atom. Scatter on the atom positions due to spatial resolution was modelled by adding a Gaussian scatter to the coordinates. A value of $2\sigma = 0.35 \text{ nm}$ for ECoTAP and $2\sigma = 0.85 \text{ nm}$ for LEAP HR for the X and Y coordinates was chosen to simulate lateral resolution (LR). A value of $2\sigma = 0.05 \text{ nm}$ for the Z coordinates was used to simulate the depth resolution (DR) (Table 1). 10 different simulations were performed for each Cr content (200 particles per Cr content). For each of the 10 simulations, the initial microstructure was the same but the generated sequence of random numbers to account for detection efficiency and spatial resolution was different.

The composition measurements were performed using erosion profile [27] on clusters identified by the iso-position method (IPM) [27,38,39]. The Cr concentration was estimated from atoms located in the core of the particle *i.e.* on the plateau appearing on the erosion profiles. The results extracted from these simulations are reported in Fig. 2. This figure presents the measured Cr concentration in α' after blurring of the lattice by lateral resolution and applying detector efficiency versus the initial Cr concentration of perfect spherical particles for both ECoTAP and LEAP HR.

As shown in Fig. 2, for high lateral resolution ($LR = 0.35 \text{ nm}$), the measured values are very close to the initial ones. As shown in Fig. 3, in this case, the lateral resolution only impacts the interface between particles and the matrix. When lateral resolution is lower ($LR = 0.85 \text{ nm}$), the Cr concentration of the particles is slightly underestimated. This underestimation ranges from $0.5 \text{ at.}\%$ to $4.6 \text{ at.}\%$ depending on the initial composition of the particles. As expected in case of lateral resolution whose value is close to the particle radius, not only the interface is affected but also the plateau (Fig. 3): the plateau is no more horizontal. This is due to the fact that the beginning of the plateau is more impacted than the core of the particles. For particles having $50 \text{ at.}\%$ Cr and $60 \text{ at.}\%$ Cr, the underestimation is in the order of magnitude of the statistical uncertainties ($\sim 0.7\text{--}0.9 \text{ at.}\%$). In case of more concentrated particles, the deviation becomes more significant. The lateral scatter due to

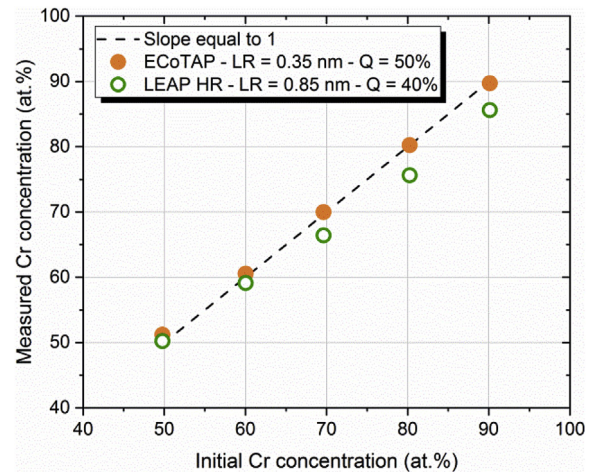


Fig. 2. Measured Cr concentration in α' after blurring of the lattice by lateral resolution and applying detection efficiency versus the initial Cr concentration for both ECoTAP and LEAP HR. On the dashed line, the measured concentrations are equal to the initial concentrations. Uncertainties are smaller than the size of the symbols (between $0.4 \text{ at.}\%$ and $0.8 \text{ at.}\%$). Uncertainties are smaller than the size of the symbols ($\sim 0.6\text{--}0.9 \text{ at.}\%$).

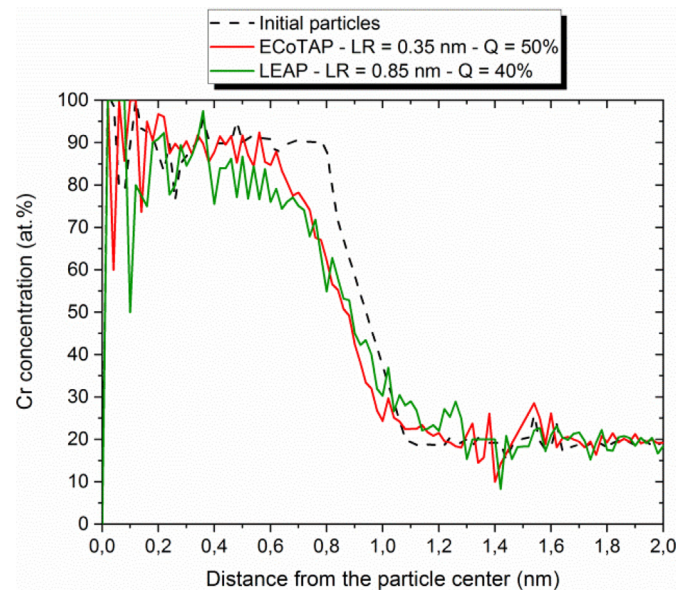


Fig. 3. Erosion profiles in Cr (at.%) starting from the particles centers before and after degradation of the data set. Initial Cr content of the particles is $90 \text{ at.}\%$ Cr.

lateral resolution impacts more the particles having a higher Cr content. This is indeed quite natural that the effect of the mixing between cluster and matrix atoms has a larger impact on the measured concentrations in the cases exhibiting the highest Cr content difference between the particles and the matrix ($19 \text{ at.}\%$). Nevertheless, it is worth noting that the dilution associated with the spatial resolution is less than $4.6 \text{ at.}\%$ in the worst case which remains relatively low. Regarding the experimental data set presented in section 2 (Fig. 1) and obtained with ECoTAP, lateral resolution and detection efficiency do not impact the measurements of the particles composition.

3.2. Local magnification

Local magnification is observed in APT experiments when two phases present different evaporation fields [40]. Because of this

difference, the steady state shape of the tip surface is different in the two phases. This leads to a modification of the ion trajectories. In Fe–Cr alloys, α' evaporation field is lower than the matrix one [41]. In such a case, a focussing of ion trajectories is observed. The trajectories of the ions of the precipitates are thus compressed leading to a compression of the precipitates in the X–Y plane and consequently to an increase in their atomic density [42]. It is important to emphasize that this increase in atomic density we just spoke about is not linked to a mixing of the atoms from the two phases but only to the compression of ion trajectories.

Because of these trajectory aberrations, trajectory overlaps may be present at the interface between particles and matrix. The amplitude of these overlaps depends on the field difference of the two phases. When the difference is small, only interfaces are affected and the core of the precipitates remains free of any matrix atoms [42]. When the difference is larger and the precipitates are small enough, the core of the precipitates may be affected and the particles and the surrounding matrix can be mixed. In the case of oxide particles (insulating phase) dispersed in a ferritic matrix one can even observe ion trajectory crossing as shown by Hatzoglou et al. [34].

In order to study the impact of the local magnification effect on the measured composition of α' particles, a numerical approach simulating field evaporation of atoms has been applied. Three major simulation models exist [43]. In this study, the model developed at the GPM by Vurpillot et al. [25,33,42,43] has been used. This model has been shown to exhibit a quantitative good agreement with experimental results in term of chemical biases induced by local magnification [34,44].

The simulated system is composed of two elements: Fe and Cr. The chemical nature of the elements is introduced in the model through their evaporation field. Assigning a different evaporation field to species rather than to phases allow us to account for chromatic effects [26]. The evaporation field of Fe (E_{Fe}) is equal to 33 V/nm [45]. This corresponds to a relative evaporation field of 0.85 (E_{Cr}/E_{Fe}). In the model, this difference is taken into account by evaporating Cr atoms under an electric field equal to 85% of the one needed to evaporate a Fe atom. Difference in composition of the phases leads to a difference in their evaporation field. As in the previous section, it has been chosen to simulate α' particles of 1 nm in radius embedded in an Fe matrix containing 19 at.% Cr. Cr content of the particles with abrupt interfaces has been set to 60 at.% (measured composition after 50 h of ageing – Fig. 1) or 84 at.% (equilibrium composition). The objective of this section is to check whether local magnification effects can introduce 24 at.% of Fe in the small particles and thus dilute them up to the level measured experimentally i.e. 60 at.% after 50 h of ageing (Fig. 1).

The simulated tip has been field evaporated using the simulation model and data were treated as the experimental data using the 3D GPM software. The isoposition method [27,38,39] has been used to identify the particles in the volume.

After field evaporation simulation, initially spherical particles are no more spherical but ellipsoidal (Fig. 4a and b) as observed experimentally (Fig. 4c) [7] and already reported in Ref. [42] for Fe–Cu. In Fig. 4, Fe and Cr atoms initially coming from the precipitates are represented together with Cr atoms of the matrix. The major axis of the ellipsoidal particle is along the evaporation direction (Z axis in Fig. 4a, b and c) and the particle compression occurs in its normal plane. The particle dimension along the evaporation direction remains unchanged as previously observed by other authors [42,43]. The shape factor $S = XY/Z^2$ (with X, Y and Z the particle dimensions along x, y and z directions) is no more equal to 1 (corresponding to a sphere). S values obtained by simulation fit well the experimental one. As a consequence of the compression, the atomic density in the particles increases.

The atomic density increase is quantified owing to profiles of relative atomic density (number density of atoms in the particle over the number density of atoms in the matrix [29]) drawn through the particles (Fig. 5). Similarly to the experimental atomic density profile, simulated profiles exhibit a reduced density close to 2. Agreement of both relative atomic density and shape factors shows the usefulness of the simulation to reproduce the local magnification effect.

Fig. 6 presents Cr erosion profiles for particles of 1 nm in radius after field evaporation. Simulations were performed on particles having the same Cr contents as the ones in Fig. 4. Atoms coming from the particles and from the matrix are distinguished. Three important conclusions can be drawn from these profiles:

- Comparison of the concentration profiles of Cr in particles before and after evaporation shows that the erosion profiles are affected by the compression of the particles due to the magnification effect: the apparent size corresponds to the shortest distance which is observed in XY plan. We will see in section 4 that this apparent size does not correspond to the actual size of the particles.
- A careful inspection of the profiles reveals that the length of the plateau is not the same for Cr and for Fe. A difference of about 0.15 nm is observed. If the level of the plateau is not modified, the plateau is systematically shorter for Cr. This chromatic effect modifies the composition of the particles. The modification is larger for particles with a larger Fe concentration. Measurement of Cr concentration of particles having an initial Cr content of 61 at.% Cr gives a Cr concentration of 65.5 at.% after evaporation. In the case of an initial concentration of 83 at.% Cr, a Cr concentration of 83.5 at.% is measured after evaporation. In both cases, composition has been measured by considering the length of the Cr plateau.

As shown in these figures, no matrix atoms enter the core of the particles. According to these simulations, local magnification effects do not introduce any matrix atoms in the particles. The amplitude of the overlap between particle atoms and those coming from the matrix is about 0.5 nm as predicted by Ref. [42]. As no matrix atoms enter the core of the particles, it is clear that the major contribution to the over atomic density is the ion focussing as already reported in Refs. [7,9]. These results rule out any artificial mixing due to local magnification effect in the core of the particle. This conclusion has also been verified using a second approach which is analytical [29,34] and presented in the next section.

3.3. The chemical composition correction (CCC) model

The analytical model was initially developed to provide the real chemical composition of nano-oxides in a ferritic matrix and was shown to work very well [29,34]. This approach is very powerful to have an idea of the type of artefact occurring during APT experiments. This model is based on the analytical expression of the reduced atomic density (ρ) in the particles. As already mentioned above, the reduced density reflects the presence or not of APT artefacts (except an eventual mixing due to lateral resolution) and is expressed as [29]:

$$\rho = \frac{V_{at}^M}{V_{at}^{Np}} \times \frac{1}{S} \left(1 + \frac{N_{Mix}}{N_R} - p^{NQ} \right) \quad (1)$$

with V_{at}^i the atomic volume of the matrix (M) or nano-particle (Np), S the particle shape factor ($S = XY/Z^2$ - with X, Y and Z the particle dimensions along x, y and z directions), N_{Mix} the number of atoms

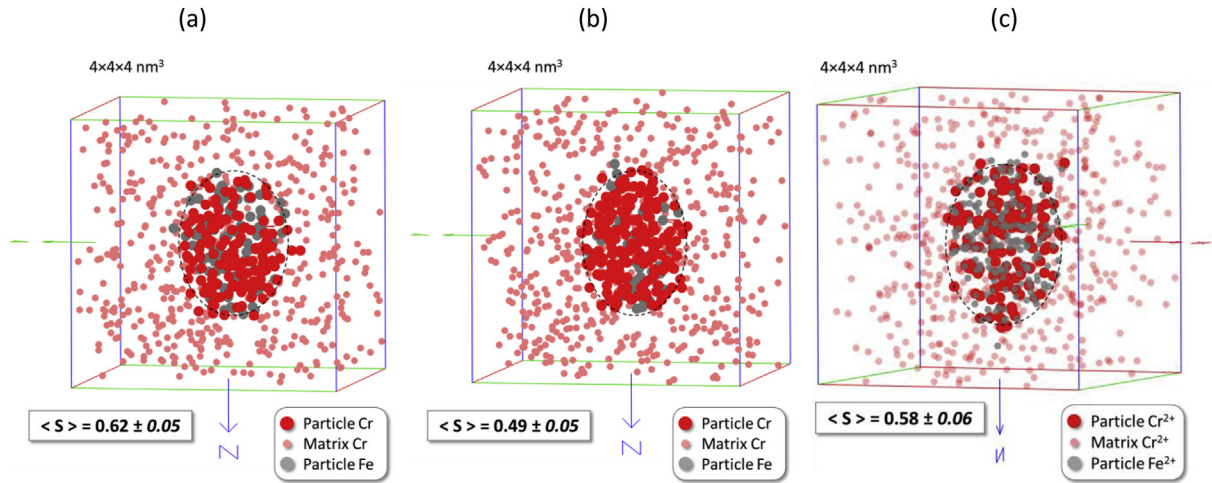


Fig. 4. Particle morphology after field evaporation simulation for a (a) 60 at.%Cr particle, (b) 84 at.% and (c) experimentally observed at 50 h. The average shape factor ($\langle S \rangle$, section 3.2) is also reported. Are shown the Cr atoms from particles (big red dots), Cr atoms from the matrix (small light red dots) and Fe from particles (grey dots). (For interpretation of the references to colour in this figure legend, the reader is referred to the Web version of this article.)

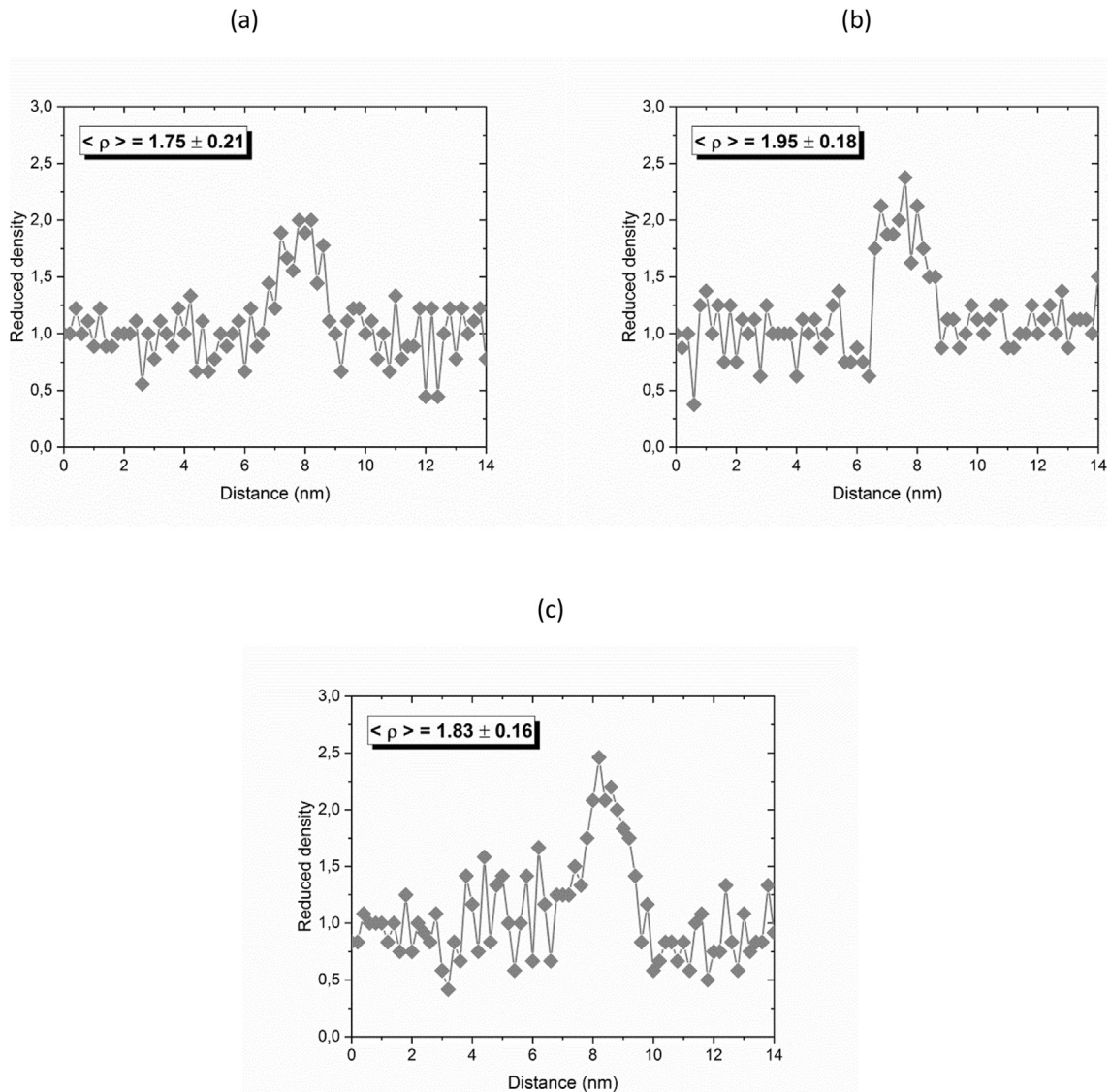


Fig. 5. Reduced atomic density profile through a particle along the evaporation direction for a simulated particle containing initially (a) 60 at.% and (b) 84 at.% of Cr and (c) for an experimental particle (50 h). It is also reported for each case the average reduced atomic density ($\langle \rho \rangle$) [29].

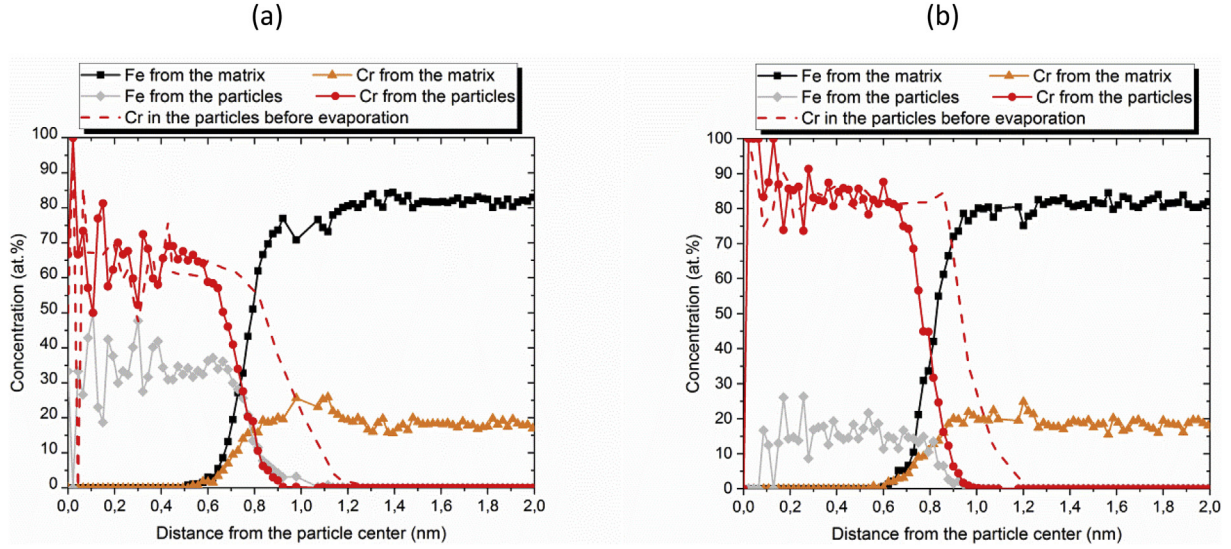


Fig. 6. Erosion profile starting from the particles center for simulated data after field evaporation simulation of particles having (a) 61 at.% and (b) 83 at.% of Cr. Atoms coming from the particles and from the matrix are distinguished. Dashed lines correspond to the Cr profiles in particles before evaporation.

introduced by trajectory overlaps in the inter-mixing zone, N_R the real number of atoms expected by APT in the particles and $p^{NQ} = N^{NQ}/N_R$ the proportion of particle atoms which are non-quantified due to APT artefacts such as preferential evaporation or molecular dissociation (with N^{NQ} the number of non-quantified atoms). The atomic volume in α' particles is equal to the one in the matrix ($V_{at}^M = V_{at}^{Np}$) [46]. Because there is no preferential evaporation in the case of α' particles, the expression (1) can be simplified to:

$$\rho = \frac{1}{S} \left(1 + \frac{N_{Mix}}{N_R} \right) \quad (2)$$

As discussed above, two contributions can lead to the observed over atomic density in α' particles:

- The focussing of ion trajectories (characterized by S). Because of the focussing, particles appear more or less ellipsoidal in APT volumes [7] and Fig. 4b) whereas they are initially spherical ($S = 1$) as confirmed by TEM observations (Fig. 7).
- The mixing of atoms coming from the particle surrounding environment (N_{Mix}).

Let's consider now two cases. In the first case, one considers that local magnification effect induces both focussing of ion trajectories

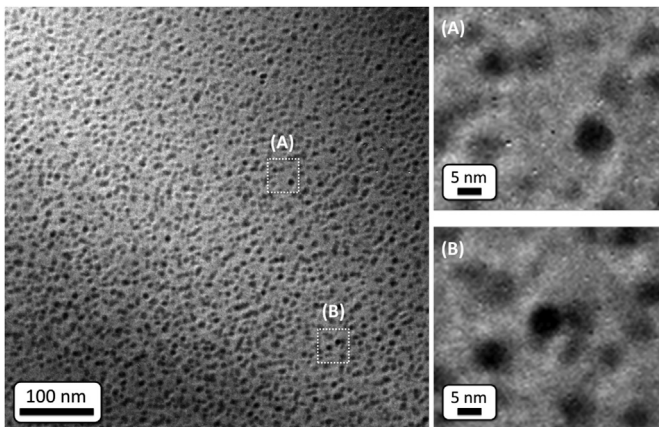


Fig. 7. TEM image in BF (Bright Field) conditions of Fe20Cr aged at 500 °C for 1067 h. Number density and size are identical to those measured with APT.

and mixing of matrix atoms with particle atoms *i.e.* one considers that actual Cr concentration is the equilibrium one (83 at.%) and that the value of 60 at.%Cr is a consequence of the mixing. The expression of equation (2) becomes:

$$\rho = \frac{1}{S} \left(1 + \frac{X_M^{Cr} - X_E^{Cr}}{X_{Mat}^{Cr} - X_M^{Cr}} \right) \quad (3)$$

with $X_E^{Cr} = 83$ at.% the α' Cr equilibrium concentration, X_M^{Cr} the Cr concentration of the particles as measured by APT and $X_{Mat}^{Cr} = 19$ at.% the Cr concentration in the matrix. The expression is obtained by considering that the atoms from the matrix are artificially introduced in the particles in the same proportion than the matrix composition, as observed by Hatzoglou et al. [29,34].

In the second case, one considers only ion focussing without any mixing. The over atomic density is thus exclusively due to trajectory focussing. The expression of equation (2) becomes in that case:

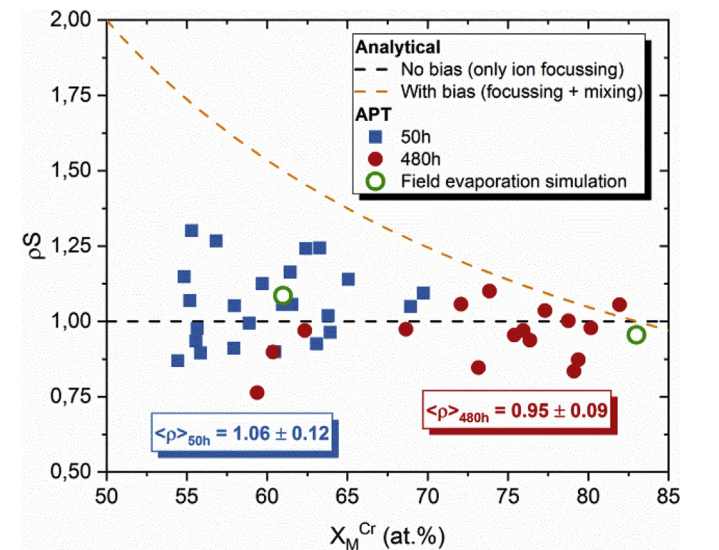


Figure 8. ρ_S as function of the Cr content (at.%) in particles 1 nm in radius measured by APT (X_M^{Cr}) together with the evolution of ρ_S as given by equations (3) and (4).

Table 2
Cr concentration (at.%) as measured with the erosion profile after field evaporation and applying a detection efficiency, a lateral resolution and a depth resolution (X_{Np}^{Cr}). X_{input} is the initial Cr content.

| X_{input} (at.%) | 61 | | 83 | |
|--|------------|------------|------------|------------|
| X_{Np}^{Cr} after evaporation | 65.5 ± 1.7 | | 83.6 ± 1.1 | |
| | ECOTAP | LEAP HR | ECOTAP | LEAP HR |
| X_{Np}^{Cr} (at.%) (after evaporation + LR) | 65.0 ± 0.8 | 61.5 ± 1.1 | 82.2 ± 0.6 | 77.8 ± 1.0 |
| Percentage of atoms coming from the matrix (at.%) | 4.0 ± 0.4 | 13.9 ± 0.8 | 4.1 ± 0.3 | 11.6 ± 0.8 |
| Particle radius deduced from the number of atoms in the particles (nm) | 1.1 ± 0.2 | 1.1 ± 0.2 | 1.1 ± 0.2 | 1.2 ± 0.2 |
| Guinier radius (nm) | 1.0 ± 0.2 | 1.0 ± 0.2 | 1.0 ± 0.2 | 1.0 ± 0.2 |

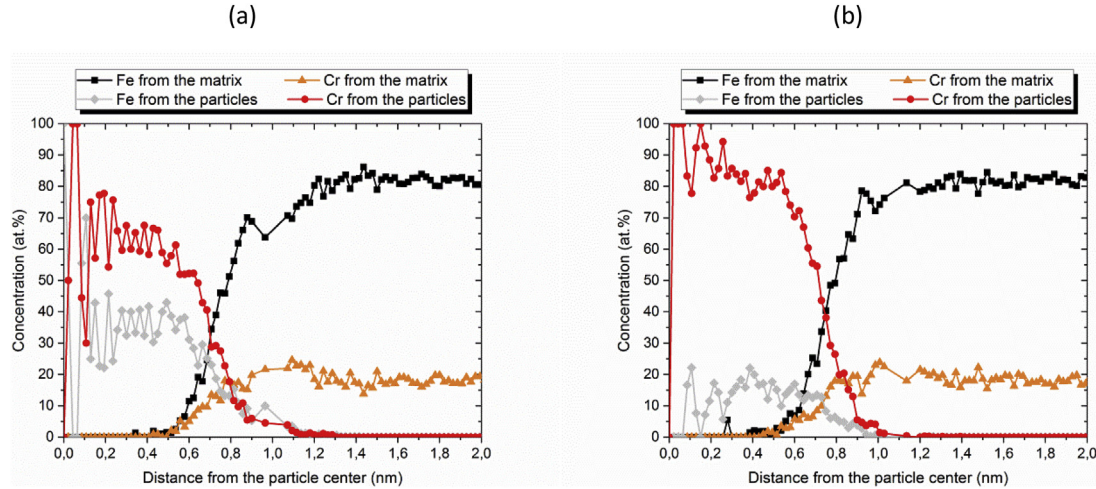


Fig. 9. Erosion profiles starting from the particle center for (a) particles having an initial Cr content of 61 at.% and (b) an initial Cr content of 84 at.%. In both case, the erosion profile was constructed on field evaporated particles after application of a LR = 0.35 nm, DR = 0.05 nm and Q = 50% (ECOTAP conditions).

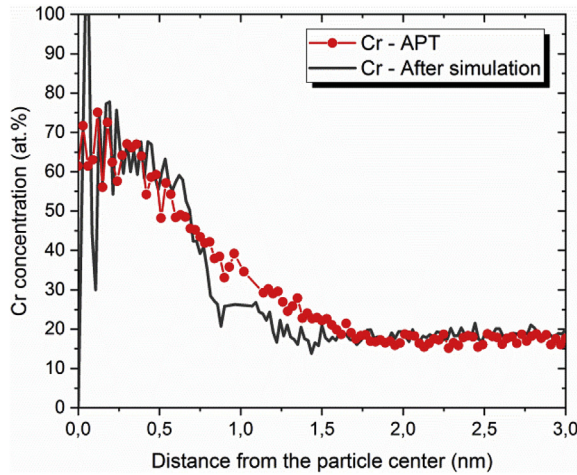


Fig. 10. Comparison of the Cr erosion profile for particles having a Cr content of 61 at.% as obtained after simulation of ECOTAP analysis with an experimental profile obtained in the Fe-20 at.% Cr aged 50 h at 500 °C.

$$\rho = \frac{1}{S} \quad (4)$$

Fig. 8 presents the evolution of ρS versus the measured Cr concentration in the particles (X_M^{Cr}) as obtained with equations (3) and (4) (dashed lines). Fig. 8 also reports the ρS values experimentally obtained after 50 h (blue diamonds) and 480 h (red

diamonds) of ageing for 1 nm particle radius. It is worth noting that at 480 h, 1 nm particles are observed with high Cr content, very close to equilibrium value. This is in favour of a kinetics origin for the different Cr contents. Are also added the values obtained by simulation of field evaporation. They agree very well with the experimental data.

Whatever the ageing time, the experimental values of ρS are distributed around the dashed line related to focussing of ions without any mixing ($\rho S = 1$ according to equation (4)). This agrees very well with the results obtained by modelling of field evaporation. Nevertheless, looking carefully, one can observe a slight shift towards upper values for 50 h of ageing. This means that a small contribution of mixing is observed.

Anyway, the error due to mixing remains low. The major contributor to over atomic density in the α' particles is the trajectory focussing. This disagrees with what some authors suggest in the literature [14–17].

4. Chemical biases due to both APT spatial resolution and local magnification effects

In order to account for both spatial resolution and local magnification effects, simulation of blurring due to spatial resolution was applied to particles that were firstly field evaporated. Parameters used for field evaporation, for spatial resolution and detection efficiency are the same as in section 3 (i.e. for ECOTAP: LR = 0.35 nm, Q = 50% and for LEAP HR: LR = 0.85 nm, Q = 40%, for both DR = 0.05 nm and $E_{Cr} = 0.85 E_{Fe}$). Simulations were performed on particles having an initial Cr content of 61 and 83 at.% Cr and a radius of 1 nm as previously. Table 2 reports the Cr content

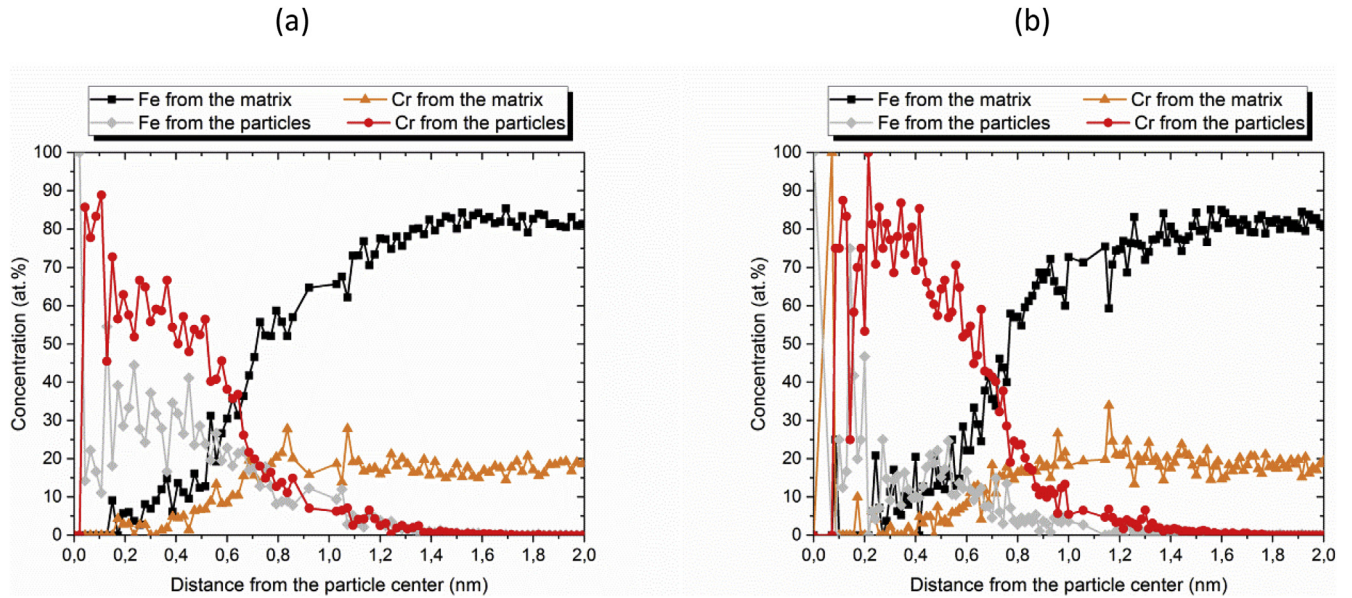


Fig. 11. Erosion profiles starting from the particle center for (a) particles having an initial Cr content of 61 at.% and (b) an initial Cr content of 84 at.%. In both case, the erosion profile was constructed on field evaporated particles after application of a LR = 0.85 nm, DR = 0.05 nm and Q = 40% (LEAP HR conditions).

measured in the particles together with the percentage of atoms originating from the matrix. In good agreement with section 3.1, the lowest the lateral resolution is, the highest is the percentage of mixing. Concentration has been measured over the length of the Cr plateau of the erosion profiles.

4.1. Simulation of ECoTAP analyses

Measurements show that 4% of matrix atoms are artificially included in the particles. As explained in section 3.1, this is due to lateral resolution. It is worth noting that 4% of matrix atoms entering the particles does not mean an error of 4% on the concentration as shown in Table 2 nor an increase of 4% of atoms in the particles. Indeed, lateral resolution effect is a random phenomenon which affects with the same probability atoms inside the particles and matrix atoms: whereas atoms from the matrix enter the particles, atoms from the particles go into the matrix (the flux is null). The effect of lateral resolution is to further smooth the interface between particles and matrix and blur the atom positions as shown in Fig. 3. As shown in Fig. 9a and 9b, matrix atoms do not enter up to the core of the particles even after the compression due to local magnification effect. Only the beginning of the plateau is affected.

In the case of particles having initially 83 at.% Cr, an underestimation of the Cr content of only 0.6 at.% is measured (1.4% if compared to the Cr content after evaporation). For particles having a lower Cr content, an excess of 4 at.% Cr is measured because of chromatic effects. If one compares to the Cr concentration measured after evaporation, an underestimation of only 0.5 at.% is noticed.

Table 2 also reports the particle radii as deduced from the number of atoms inside the particles and the Guinier radius. The interface between particles and matrix is placed at inflection point of the erosion profile. These radii are similar and close to the particle radius of the input particles. It is worth noting that calculation of the radius must not be done directly on erosion profile. Indeed the erosion profile is affected by the compression of the particles due to the magnification effect: the apparent size corresponds to the shortest distance which is observed in XY plan.

Fig. 10 compares a Cr erosion profile as obtained after simulation of ECoTAP analysis of particles having a Cr content of 61 at.% with an

experimental profile obtained in the Fe-20 at.% Cr aged 50 h at 500 °C. The simulation very well reproduces the plateau of the experimental profile (see Fig. 10).

These results show that it is not possible for α' particles having the Cr equilibrium concentration and a radius of 1 nm to become, after APT analysis with an ECoTAP (as in the study of Novy et al. [7]), particles containing only 60 at.% because of the APT spatial resolution and local magnification effect. 60 at.% Cr observed at the beginning of the kinetics cannot be a consequence of APT artefacts as reported by Novy et al. and Kuksenko et al. [7,9] and recently by Reese et al. [24].

4.2. Simulation of LEAP HR analyses

Table 2 reports the Cr concentration measured after applying a LR equal to 0.85 nm, a DR of 0.05 nm and a detector efficiency of 40% as for LEAP HR analyses. The number of matrix atoms entering the particles becomes more significant (between 11% and 14%) because of the lowest lateral resolution. As already mentioned in section 3.1, with this lateral resolution, the matrix atoms reach the core of the particles leading to an underestimation of the Cr content (Fig. 11). This underestimation is slightly larger after evaporation because of the compression in the XY plan due to the local magnification effect (for comparisons see section 3.1).

As previously and for the same reason, the particle radius is not impacted. Nevertheless, it is not the case for the composition. As observed when only lateral scatter applies, composition of particles having 83 at.% Cr is much more impacted than composition of particles containing 61 at.%. In the former case, an underestimation of 5.2 at.% is observed. However, the underestimation remains low. Of course, it will be increased for system with a larger concentration contrast between particles and matrix. Nevertheless, in the case of the system investigated here, even with the worse lateral resolution, the 60 at.% Cr observed at the beginning of the kinetics cannot be a consequence of APT artefacts. Again, it must be emphasized that, according to the simulations and calculations performed in this study, this dilution is mainly due to the lateral resolution of APT and not to the local magnification effect. These results agree well with theory [19,22,23]: variation of Cr content of

particles with the radius is not an APT artefact but has kinetic/thermodynamic origin(s) for particle radius larger than 1 nm. However, we have to keep in mind that the Cr content may be underestimated up to 5 at.%, the underestimation varying with the concentration contrast between particles and matrix and the atom probe used.

5. Conclusion

In this study, the impact of APT spatial resolution and local magnification effect on the chemical composition measurements of α' particles of 1 nm in radius has been quantified. These phenomena are the two major contributors to chemical biases linked to APT experiments in the case of Fe–Cr alloys. Influence of APT spatial resolution has been estimated using the numerical approach presented in Ref. [28]. Local magnification effect quantification was performed by two methods: modelling of field evaporation using the method developed by Vurpillot et al. [25,32,33] and by using the CCC analytical model of Hatzoglou et al. [29,34].

The results showed that:

- The dilution associated with the spatial resolution is less than 0.4 at.% for an APT having a lateral resolution of 0.35 nm (spatial resolution of ECoTAP). It varies from 0.5 to 4.6 at.% when lateral resolution equals 0.85 nm (spatial resolution of LEAP HR). The lower the Cr content of the particles is, the lower is the dilution of small particles due to APT lateral resolution.
- The major effect of local magnification is ion focussing with no mixing in the core of the particles. Simulation showed that the inter-mixing region is located at the interface of the particles without degrading the core composition. The major contribution to the over atomic density in particles is thus the focussing of ion trajectories and not atoms coming from the matrix. Simulation of field evaporation has revealed the existence of chromatic effects which results in an increase in the apparent Cr content of particles. The effect is larger for particles having more Fe.
- Taking into account both spatial resolution and local magnification effects showed that for high lateral resolution, matrix atoms do not enter up to the core of the particles even after the compression due to local magnification effect. The effect of lateral resolution is only to further smooth the interface between particles and matrix and to affect the beginning of the plateau. For lower lateral resolution, matrix atoms reach the core of the particles leading to an underestimation of the Cr content as expected in case of lateral resolution whose value is close to the particle radius. Underestimation of the Cr content is only 0.6 at.% for ECoTAP and 5.2 at.% for LEAP HR in the case of particles having initially 83 at.% Cr. For particles having a lower Cr content (61 at.%) significant chromatic effects have been revealed. These effects lead to an increase in Cr content of 4.5 at.% in the particles. Consequently, even with the scatter introduced by the lateral resolution, an excess of 4 at.% Cr is measured for ECoTAP and 1.5 at.% for LEAP HR.
- Local magnification effect has less impact on composition measurements than lateral resolution.
- These results show that it is not possible for α' particles having the Cr equilibrium concentration and a radius of 1 nm to become, after APT analysis, particles containing only 60 at.% because of the APT spatial resolution and local magnification effect. A maximum underestimation of 5.2 at.% is expected. By investigating only effect of APT limitations, this work enabled to separate APT limitations from kinetics/thermodynamic effect on the Cr content of small particles.

Acknowledgements

The authors acknowledge F. Vurpillot for fruitful discussion.

Appendix A. Supplementary data

Supplementary data to this article can be found online at <https://doi.org/10.1016/j.jnucmat.2019.05.022>.

References

- [1] F.A. Garner, M.B. Toloczko, B.H. Sencer, Comparison of swelling and irradiation creep behavior of fcc-austenitic and bcc-ferritic/martensitic alloys at high neutron exposure, *J. Nucl. Mater.* 276 (2000) 123–142, [https://doi.org/10.1016/S0022-3115\(99\)00225-1](https://doi.org/10.1016/S0022-3115(99)00225-1).
- [2] R.L. Klueh, *High-chromium Ferritic and Martensitic Steels for Nuclear Applications*, ASTM, W., Conshohocken, PA, 2001.
- [3] E.A. Little, Development of radiation resistant materials for advanced nuclear power plant, *Mater. Sci. Technol.* 22 (2006) 491–518, <https://doi.org/10.1179/174328406X90998>.
- [4] A. Kohyama, A. Hishinuma, D.S. Gelles, R.L. Klueh, W. Dietz, K. Ehrlich, Low-activation ferritic and martensitic steels for fusion application, *J. Nucl. Mater.* 233–237 (1996) 138–147, [https://doi.org/10.1016/S0022-3115\(96\)00327-3](https://doi.org/10.1016/S0022-3115(96)00327-3).
- [5] M. Matijasevic, A. Almazouzi, Effect of Cr on the mechanical properties and microstructure of Fe–Cr model alloys after n-irradiation, *J. Nucl. Mater.* 377 (2008) 147–154, <https://doi.org/10.1016/j.jnucmat.2008.02.061>.
- [6] F. Bergner, C. Pareige, M. Hernández-Mayoral, L. Malerba, C. Heintze, Application of a three-feature dispersed-barrier hardening model to neutron-irradiated Fe–Cr model alloys, *J. Nucl. Mater.* 1–3 (2014) 96–102, <https://doi.org/10.1016/j.jnucmat.2014.01.024>.
- [7] S. Novy, P. Pareige, C. Pareige, Atomic scale analysis and phase separation understanding in a thermally aged Fe–20at.%Cr alloy, *J. Nucl. Mater.* 384 (2009) 96–102, <https://doi.org/10.1016/j.jnucmat.2008.10.008>.
- [8] F. Bley, Neutron small-angle scattering study of unmixing in Fe–Cr alloys, *Acta Metall. Mater.* 40 (1992) 1505–1517, [https://doi.org/10.1016/0956-7151\(92\)90094-U](https://doi.org/10.1016/0956-7151(92)90094-U).
- [9] V. Kuksenko, C. Pareige, C. Genevois, F. Cuvilly, M. Roussel, P. Pareige, Effect of neutron-irradiation on the microstructure of a Fe–12at.%Cr alloy, *J. Nucl. Mater.* 415 (2011) 61–66, <https://doi.org/10.1016/j.jnucmat.2011.05.042>.
- [10] F. Bergner, C. Pareige, V. Kuksenko, L. Malerba, P. Pareige, A. Ulbricht, A. Wagner, Critical assessment of Cr-rich precipitates in neutron-irradiated Fe–12at.%Cr: comparison of SANS and APT, *J. Nucl. Mater.* 442 (2013) 463–469, <https://doi.org/10.1016/j.jnucmat.2013.05.023>.
- [11] V. Kuksenko, C. Pareige, P. Pareige, Cr precipitation in neutron irradiated industrial purity Fe–Cr model alloys, *J. Nucl. Mater.* 432 (2013) 160–165, <https://doi.org/10.1016/j.jnucmat.2012.07.021>.
- [12] O. Tissot, C. Pareige, E. Meslin, B. Decamps, J. Henry, Kinetics of α' precipitation in an electron-irradiated Fe15Cr alloy, *Scripta Mater.* 122 (2016) 31–35, <https://doi.org/10.1016/j.scriptamat.2016.05.021>.
- [13] O. Tissot, C. Pareige, E. Meslin, B. Decamps, J. Henry, Influence of injected interstitials on α' precipitation in Fe–Cr alloys under self-ion irradiation, *Mater. Res. Lett.* 5 (2017) 117–123, <https://doi.org/10.1080/21663831.2016.1230896>.
- [14] M. Bachhav, G. Robert Odette, E.A. Marquis, α' precipitation in neutron-irradiated Fe–Cr alloys, *Scripta Mater.* 74 (2014) 48–51, <https://doi.org/10.1016/j.scriptamat.2013.10.001>.
- [15] W.-Y. Chen, Y. Miao, Y. Wu, C.A. Tomchik, K. Mo, J. Gan, M.A. Okuniewski, S.A. Maloy, J.F. Stubbs, Atom probe study of irradiation-enhanced α' precipitation in neutron-irradiated Fe–Cr model alloys, *J. Nucl. Mater.* 462 (2015) 242–249, <https://doi.org/10.1016/j.jnucmat.2015.04.005>.
- [16] S.A. Briggs, P.D. Edmondson, K.C. Littrell, Y. Yamamoto, R.H. Howard, C.R. Daily, K.A. Terrani, K. Sridharan, K.G. Field, A combined APT and SANS investigation of α' phase precipitation in neutron-irradiated model FeCrAl alloys, *Acta Mater.* 129 (2017) 217–228, <https://doi.org/10.1016/j.actamat.2017.02.077>.
- [17] P.D. Edmondson, S.A. Briggs, Y. Yamamoto, R.H. Howard, K. Sridharan, K.A. Terrani, K.G. Field, Irradiation-enhanced α' precipitation in model FeCrAl alloys, *Scripta Mater.* 116 (2016) 112–116, <https://doi.org/10.1016/j.scriptamat.2016.02.002>.
- [18] P.E. L'vov, V.V. Svetukhin, A.V. Obukhov, Thermodynamics of phase equilibrium of binary alloys containing nanoprecipitates, *Phys. Solid State* 53 (2011) 421–427, <https://doi.org/10.1134/S1063783411020156>.
- [19] V. Svetukhin, P. L'vov, E. Gaganiidze, M. Tikhonchev, C. Dethloff, Kinetics and thermodynamics of Cr nanocluster formation in Fe–Cr system, *J. Nucl. Mater.* 415 (2011) 205–209, <https://doi.org/10.1016/j.jnucmat.2011.06.005>.
- [20] C. Zhang, M. Enomoto, Study of the influence of alloying elements on Cu precipitation in steel by non-classical nucleation theory, *Acta Mater.* 54 (2006) 4183–4191, <https://doi.org/10.1016/j.actamat.2006.05.006>.
- [21] C. Zhang, M. Enomoto, T. Yamashita, N. Sano, Cu precipitation in a prestrained Fe–1.5 wt pct Cu alloy during isothermal aging, *Metall. Mater. Trans. A* 35 (2004) 1263–1272, <https://doi.org/10.1007/s11661-004-0300-8>.

- [22] Y. Li, S.Y. Hu, L. Zhang, X. Sun, Non-classical nuclei and growth kinetics of Cr precipitates in FeCr alloys during ageing, *Acta Mater.* (2014), <https://doi.org/10.1088/0965-0393/22/2/025002>, 222Article No 025002.
- [23] J.W. Cahn, J.E. Hilliard, Free energy of a nonuniform system. III. Nucleation in a two-component incompressible fluid, *J. Chem. Phys.* 31 (1959) 688–699, <https://doi.org/10.1063/1.1730447>.
- [24] E.R. Reese, M. Bachhav, P. Wells, T. Yamamoto, G. Robert Odette, E.A. Marquis, On α' precipitate composition in thermally annealed and neutron-irradiated Fe-9-18Cr alloys, *J. Nucl. Mater.* 500 (2018) 192–198, <https://doi.org/10.1016/j.jnucmat.2017.12.036>.
- [25] D. Blavette, F. Vurpillot, P. Pareige, A. Menand, A model accounting for spatial overlaps in 3D atom-probe microscopy, *Ultramicroscopy* 89 (2001) 145–153, [https://doi.org/10.1016/S0304-3991\(01\)00120-6](https://doi.org/10.1016/S0304-3991(01)00120-6).
- [26] E.A. Marquis, F. Vurpillot, Chromatic aberrations in the field evaporation behavior of small precipitates, *Microsc. Microanal.* 14 (2008) 561–570, <https://doi.org/10.1017/S1431927608080793>.
- [27] W. Lefebvre, F. Vurpillot, X. Sauvage, *Atom Probe Tomography: Put Theory into Practice*, Elsevier, Boston, MA, 2016.
- [28] J.M. Hyde, G. DaCosta, C. Hatzoglou, H. Weekes, B. Radiguet, P.D. Styman, F. Vurpillot, C. Pareige, A. Etienne, G. Bonny, N. Castin, L. Malerba, P. Pareige, Analysis of radiation damage in light water reactors: comparison of cluster analysis methods for the analysis of atom probe data, *Microsc. Microanal.* 23 (2017) 366–375, <https://doi.org/10.1017/S1431927616012678>.
- [29] C. Hatzoglou, B. Radiguet, P. Pareige, Experimental artefacts occurring during atom probe tomography analysis of oxide nanoparticles in metallic matrix: quantification and correction, *J. Nucl. Mater.* 492 (2017) 279–291, <https://doi.org/10.1016/j.jnucmat.2017.05.008>.
- [30] J. Takahashi, K. Kawakami, A quantitative model of preferential evaporation and retention for atom probe tomography, *Surf. Interface Anal.* 46 (2014) 535–543, <https://doi.org/10.1002/sia.5555>.
- [31] J. Takahashi, K. Kawakami, D. Raabe, Comparison of the quantitative analysis performance between pulsed voltage atom probe and pulsed laser atom probe, *Ultramicroscopy* 175 (2017) 105–110, <https://doi.org/10.1016/j.ultramic.2017.01.015>.
- [32] F. Vurpillot, A. Cerezo, D. Blavette, D.J. Larson, Modeling image distortions in 3DAP, *Microsc. Microanal.* 10 (2004) 384–390, <https://doi.org/10.1017/S1431927604040486>.
- [33] M. Gruber, F. Vurpillot, A. Bostel, B. Deconihout, Field evaporation: a kinetic Monte Carlo approach on the influence of temperature, *Surf. Sci.* 605 (2011) 2025–2031, <https://doi.org/10.1016/j.susc.2011.07.022>.
- [34] C. Hatzoglou, B. Radiguet, F. Vurpillot, P. Pareige, A chemical composition correction model for nanoclusters observed by APT - application to ODS steel nanoparticles, *J. Nucl. Mater.* 505 (2018) 240–248, <https://doi.org/10.1016/j.jnucmat.2018.03.057>.
- [35] S.M. Dubiel, G. Inden, Miscibility gap in the Fe-Cr system: a moessbauer study on long term annealed alloys, *ChemInform* 18 (1987) no-no.
- [36] H. Kuwano, Mössbauer effect study on the miscibility gap of the iron-chromium binary system, *Trans. Jpn. Inst. Met.* 26 (1985) 473–481.
- [37] M.K. Miller, *Atom Probe Tomography: Analysis at the Atomic Level*, Springer US, 2000.
- [38] C. Pareige, V. Kuksenko, P. Pareige, Behaviour of P, Si, Ni impurities and Cr in self ion irradiated Fe-Cr alloys – comparison to neutron irradiation, *J. Nucl. Mater.* 456 (2015) 471–476, <https://doi.org/10.1016/j.jnucmat.2014.10.024>.
- [39] E. Meslin, B. Radiguet, M. Loyer-Prost, Radiation-induced precipitation in a ferritic model alloy: an experimental and theoretical study, *Acta Mater.* 61 (2013) 6246–6254.
- [40] M.K. Miller, M.G. Hetherington, Local magnification effects in the atom probe, *Surf. Sci.* 246 (1991) 442–449, [https://doi.org/10.1016/0039-6028\(91\)90449-3](https://doi.org/10.1016/0039-6028(91)90449-3).
- [41] M. Miller, J. Hyde, M. Hetherington, A. Cerezo, G. Smith, C. Elliott, Spinodal decomposition in Fe-Cr alloys: experimental study at the atomic level and comparison with computer models—I. Introduction and methodology, *Acta Metall. Mater.* 43 (1995) 3385–3401.
- [42] F. Vurpillot, A. Bostel, D. Blavette, Trajectory overlaps and local magnification in three-dimensional atom probe, *Appl. Phys. Lett.* 76 (2000) 3127–3129, <https://doi.org/10.1063/1.126545>.
- [43] F. Vurpillot, C. Oberdorfer, Modeling atom probe tomography: a review, *Ultramicroscopy* 159 (2015) 202–216, <https://doi.org/10.1016/j.ultramic.2014.12.013>.
- [44] C. Hatzoglou, Quantification et correction des biais inhérents à l'analyse par sonde atomique tomographique des nanoparticules d'un acier ODS: Application à l'étude de leur formation et à leur comportement sous irradiation, Ph.D., Université de Rouen, 2015.
- [45] T.T. Tsong, *Atom-Probe Field Ion Microscopy: Field Ion Emission, and Surfaces and Interfaces at Atomic Resolution*, Cambridge University Press, 2005.
- [46] P. Olsson, *Ab initio* study of Cr interactions with point defects in bcc Fe, *Phys. Rev. B* 75 (2007), <https://doi.org/10.1103/PhysRevB.75.014110>.